communications earth & environment

Article

https://doi.org/10.1038/s43247-024-01794-w

Climate induced microbiome alterations increase cadmium bioavailability in agricultural soils with pH below 7

Sören Drabesch[1,2,3], Oliver J. Lechtenfeld[4,5], Esmira Bibaj[1,3], José M. León Ninin[6], Juan Lezama Pachecco[7], Scott Fendorf[7], Britta Planer-Friedrich[6], Andreas Kappler[2] & E. Marie Muehe[1,3] ✉

Climate change and metals independently stress soil microbiomes, but their combined effects remain unresolved. Here we show that future climate affects soil cadmium through altered soil microbiome and nutrient cycles, with soil pH as critical factor. In soils with pH<7 and during summer temperatures, future climate increased porewater cadmium, shifting total and potentially active taxonomic microbiome structures. Microbial ammonium oxidation released protons liberating cadmium through cation exchange from mineral surfaces. When porewater cadmium levels became toxic to non-cadmium-tolerant bacteria, microbial activity, and nutrient cycling decreased, reducing carbon and nitrogen emissions. In contrast, pH>7 soil show no climate impacts on cadmium mobilization, though imprints on microbiome structure were apparent. Subsequent nutrient cycling increased under future climate, stimulating soil respiration and nitrous oxide release. These findings underscore complex interactions between climate change and soil contaminants affecting the soil microbiome and its activity and highlights potential impacts on crop production, groundwater quality, and climate feedback.

Taxonomically and functionally diverse soil microbiomes are indispensable for agricultural productivity under global food demands[1–10]. Nevertheless, environmental stresses, such as climate change and metal contamination, can compromise soil health and microbial dynamics[11,12]. Metals, like the common cation contaminant cadmium (Cd), naturally occur at background quantities in all soils[13], but are rising due to intensified cultivation, and (legacy) atmospheric depositions due to mining or industry[14]. Cadmium holds no known metabolic function[15], is considered toxic to any life form by inhibiting physiological processes in cells[16–18], and ranked at position seven by the Agency for Toxic Substances and Disease Registry. *Yet*, moderate concentrations have been observed to stimulate microbial growth[19] and activity[8,9,19], which is likely due to a stress response that enhances metabolic processes[19] and the activation of defense mechanisms[9]. Whether soil biota is affected or not by heavy-metal-related toxicity depends on the bioavailable fraction (i.e., dissolved or weakly adsorbed), rather than the total concentration[18,20]. Metal bioavailability is governed by pH, organic matter content and composition, and the type of minerals present. However, climatic conditions also play a crucial role, not only by affecting these soil properties[21] but also by impacting microbial communities[5] and mineral solubility[22]. Current evidence suggests that elevated temperature increases physical Cd retention[23,24], whereas impacts of increased atmospheric CO_2 or changes in soil moisture have yet to be considered. Earth's changing climate with shifts in the partial pressure of CO_2, temperature, and precipitation frequency and intensity has been investigated extensively for impacts on microbial community composition, abundance, activity, and function[5,11] Elevated temperature generally enhances microbial activity[6,11,25], while evaporation decreases soil moisture exerting drought stress on microorganisms[7]. For elevated atmospheric CO_2, contrasting findings were reported with more studies observing an increase[2,26], and less of a decrease[27], in microbial activity. While there is a growing body of research examining

[1]Plant Biogeochemistry, Department of Geosciences, University of Tuebingen, 72076 Tuebingen, Germany. [2]Geomicrobiology, Department of Geosciences, University of Tuebingen, 72076 Tuebingen, Germany. [3]Plant Biogeochemistry, Department for Applied Microbial Ecology, UFZ – Helmholtz Centre for Environmental Research, 04318 Leipzig, Germany. [4]BioGeoOmics, Department of Analytical Chemistry, UFZ – Helmholtz Centre for Environmental Research, 04318 Leipzig, Germany. [5]ProVIS – Centre for Chemical Microscopy, UFZ – Helmholtz Centre for Environmental Research, 04318 Leipzig, Germany. [6]Environmental Geochemistry, Bayreuth Center for Ecology and Environmental Research (BAYCEER), University of Bayreuth, 95447 Bayreuth, Germany. [7]Soil and Environmental Biogeochemistry, Stanford University, Stanford, CA, 94305, USA. ✉e-mail: marie.muehe@ufz.de

the singular effects of climate change or metals on the microbiome, there is a lack of studies investigating the combined impacts of these factors on soil microbiomes and the interplay between climate-induced microbiome alterations affecting Cd bioavailability. Understanding this relationship is crucial, as it directly influences the resilience of the global food system and the broader ecosystem[28,29].

Here, we evaluated the combined impacts of soil Cd and climate change on Cd bioavailability and microbial community dynamics in agricultural soils as a proof of concept study. Three European agricultural soils were examined under a multifactorial design of the two stressors (Supplementary Fig. S1 and Supplementary Table S1). The soils' native Cd content under 0.2 mg Cd kg^{-1} dry soil represents uncontaminated soils (termed low Cd). To vary total soil Cd contents, each soil was additionally amended with two Cd amounts: +0.3 (termed moderate Cd) and +2.2 mg Cd kg^{-1} dry soil (termed high Cd) (Supplementary Table S1). Moderate Cd mimicked subtle contamination, embodying ~80% of European and US topsoils[13,30], while high Cd represented contaminated areas sparsely used for food production but relevant for bioenergy production[13,30,31]. Given that the soils were from a similar climatic region and parent rock, soil pH is isolated as the primary geochemical variable in this study. Soil pH ranged from 6.3, 6.7 to 7.3, which falls into the pH range suitable to most cultivated crops[32,33] and should cover the pH ranges of at least 40% of (agricultural) soils[34,35]. In these soils, cadmium transitions from an increased mobility in the porewater to almost all Cd adsorbed to SOM and minerals, respectively[36]. Incubated in columns in exterior climatic controlled chambers with day and night temperature cycles of a marine west coast climate (Cfb)[37], soils were exposed to ambient and projected future climatic conditions. Future conditions simulated in the study considered a worst-case scenario, comparing current CO_2 levels of 430 ppm_v and temperatures with projected values of 800 ppm_v and elevated temperature by 4 °C respective to ambient temperature for the year 2100[38–40], with Liu & Raftery, 2021 proposing the current trajectory for a temperature rise until 2100 between 2.1 and 3.9 °C[41]. Under both climatic conditions, soils were irrigated with sterilized artificial rainwater at fixed intervals. Thus, soils exposed to future climatic conditions experienced lower minimum water contents between irrigations due to higher evaporative losses (Supplementary Fig. S2).

Results

Climate impact on soil cadmium

For pH 6.3 soils with a low Cd content, average porewater Cd was approximately 0.11 ug L^{-1} under today's climatic conditions, stabilizing after 35 days (Fig. 1A, Supplementary Table S2, Supplementary Fig. S3). Future climatic conditions significantly raised average porewater Cd to approximately 0.16 ug L^{-1}, being 45% higher during summer temperatures above 20 °C (Supplementary Fig. S2). Moderate and high Cd amendment disproportionally increased porewater Cd to respective 1.03 and 8.30 ug L^{-1} as amended Cd associated to mineral surfaces rather than interiors[17]. Future conditions caused significant 40% and 27% increases in porewater Cd, respectively, comparable to low and moderate Cd soils. According to a geochemical model[42] climatic conditions did not affect the relative contribution of DOC association versus free Cd^{2+} in the porewater (Supplementary Table S3). Observed climatic impacts on Cd porewater imprinted also in 0.01 M $CaCl_2$- and 0.1 M HCl-extractable Cd (Supplementary Fig. S4A–F) and in more pronounced shifts from mineral-associated to organic-bound Cd associations according to Cd K-edge EXAFS (Supplementary Fig. S5).

For soils with a higher pH, lower porewater Cd concentrations were observed and expected[43] (Fig. 1C, D, Supplementary Table S2, Supplementary Fig. S3D, E, and Supplementary Fig. S4G–I), as Cd can additionally be incorporated in the crystal structure of carbonates as an impurity[18,44] and

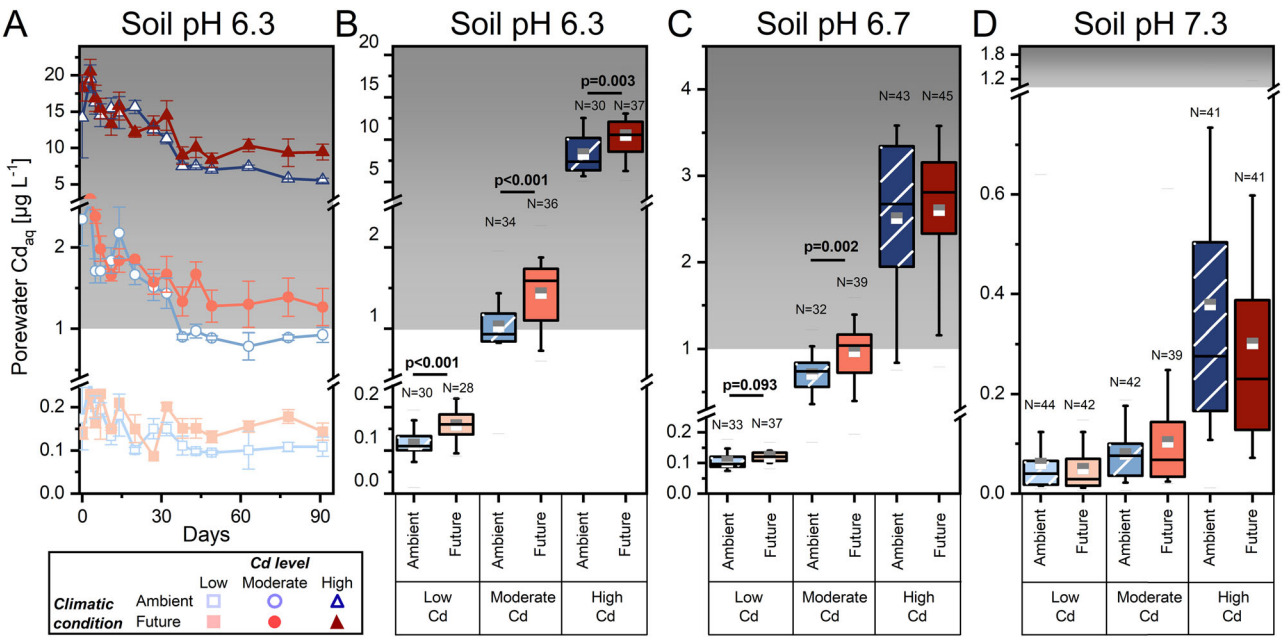

Fig. 1 | Porewater cadmium concentration in agricultural soils exposed to different climatic conditions. Porewater Cd concentration across an entire incubation season for three agricultural soils with varying pH: (**A**, **B**) pH 6.3, (**C**) pH 6.7, and (**D**) pH 7.3; and three different total soil Cd contents (low, moderate and high; for exact Cd contents per soil see Supplementary Table S1)). Please note the difference in y-axes scale due to soil pH impacts on overall porewater Cd levels. The data for the soil with pH 6.3 is only shown for the warm period after day 30 of the season as microbial impacts on porewater Cd at lower temperatures found in spring are less pronounced. The grey shaded area highlights aqueous Cd concentrations above 1 µg L^{-1}, relating to roughly the porewater concentration at which Cd toxicity outweighs Cd stimulation effects on the microbiome. Soils were exposed to ambient (430 ppm_v CO_2 and ambient temperature) and future (800 ppm_v CO_2 and +4 °C in atmospheric temperature respective to the ambient set-up) climatic conditions. Biological replicates: A, B = 5, C = 4, and D = 3 with B = 7, C = 10, and D = 15 timepoints across season. Squares represent the mean and the line in the box the median; whiskers give the Q10 and Q90, and N the number of datapoints per whisker plot. Significant differences are indicated with p-values above plots. All p-values can be found in Supplementary Table S2. Results of a generalized mixed linear model of individual and interactive effects on porewater Cd are shown in Supplementary Table S10.

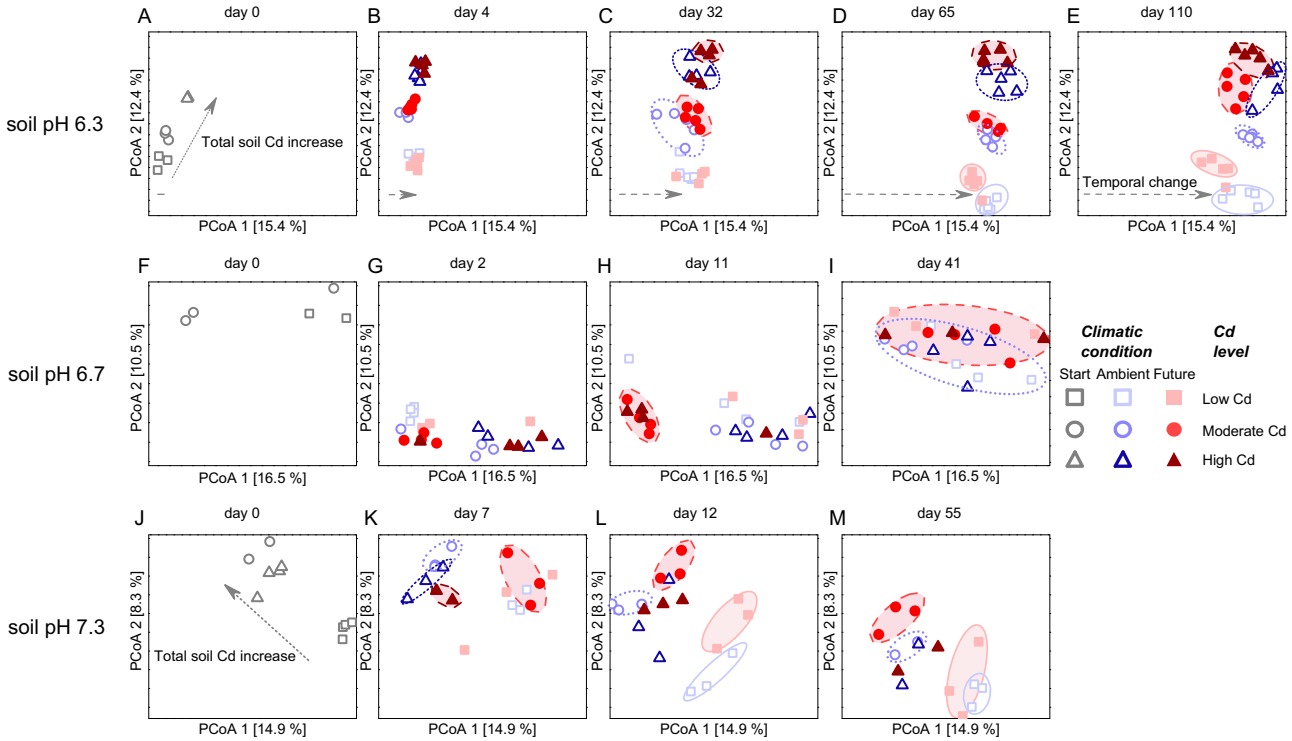

Fig. 2 | Principal coordinates analysis (PCoA) visualizing compositional whole bacterial and archaeal community differences in Cd-bearing agricultural soils exposed to different climatic conditions. PcoAs are based on 16S rDNA-calculated Bray-Curtis dissimilarities and the first two principal coordinates are displayed for three different agricultural soils with varying pH; (**A**–**E**) soil pH 6.3, (**F**–**I**) soil pH 6.7 and (**J**–**M**) soil pH 7.3 and three different total soil Cd contents (low (square), moderate (circle) and high (triangle); for exact Cd contents per soil see Supplementary Table S1) across incubation time. The soils were exposed to ambient (430 ppm_v CO_2 and ambient temperature) (blue) and future (800 ppm_v CO_2 and +4 °C in atmospheric temperature respective to the ambient setup) (red) climatic conditions. Grey arrows in (**A**) through (**E**) indicate a community shift along the PCoA 1 coordinate due to time. Colored circles indicate community shifts due to climate. PCoA was calculated for each soil independently considering all time points and respective biological replication (soil pH 6.3 = 5, soil pH 6.8 = 4, and soil pH 7.3 = 3). Average distance matrices are provided in Supplementary Table S4 for soil pH 6.3. Data points with low sequencing depth were sorted out leading to less replication for some time points (*Methods*).

less H_3O^+ ions compete for binding sites on SOM or oxide minerals. For the pH 6.7 soil, porewater Cd remained below 4 µg L^{-1} upon amendment and significantly increased by 20 and 40% in low and moderate Cd soil after 9 days of future conditions. No statistically significant increase in porewater Cd was observed for the high Cd soil, though a distinct increased trend is seen in the time-resolved data. With the pH 7.3 soil containing carbonates (Supplementary Table S1), porewater Cd remained below 1.0 ug L^{-1} with no observable climatic impact.

Alterations of the soil microbiome

Cadmium addition, after a 14-week acclimatization period before climate onset, distinctly altered total and active microbial communities on phyla and genera levels (Fig. 2A, F, J, Supplementary Fig. S6A, F, J, Supplementary Table S4 *with increasing distances*, Supplementary Fig. S7A, and Supplementary Fig. S8A). For pH 6.3 soils, Cd amendment caused a stepwise divergence to significantly different potentially active and total microbiomes, while it developed to similar degrees in the pH 7.3 soil upon Cd amendment (indicated by arrows in Fig. 2A, J and Supplementary Fig. S6A, J; highlighted in red in Supplementary Table S4). Broad community descriptors and 16S rRNA gene and transcript copy numbers indicated recovery of microbiomes from Cd amendment after 14-week acclimatization (Supplementary Fig. S9). Universally increasing or decreasing trends for phyla across all soils were not identifiable, though trends within each soil were consistent with increasing soil Cd contents pointing to metal tolerance/stimulation[45] and resistance genes[46] (Supplementary Fig. S7A, Supplementary Fig. S8A, Supplementary Tables S5–7).

Upon imposing future climatic conditions, compositional differences in taxonomic and potentially active microbial diversity evolved for all soils and Cd contents (*indicated by grey dashed arrows on the PCoA 1 coordinate and blue and red circles in* Fig. 2, Supplementary Fig. S6). Notably, a distinct separation of microbial communities due to climate was observed at day 32 of the pH 6.3 soil, becoming more pronounced over time. The degree of development after 110 days relative to day 0 was significantly further for the ambient compared to the future climate (indicated by yellow, green, and blue color-coding in Supplementary Table S4). Differences between communities exposed to ambient and future conditions were particularly significant for the two Cd treatments compared to the low Cd soil (indicated by grey color-coding in Supplementary Table S4). For the pH 6.7 soil, separation occurred at day 11 for future communities in moderate and high Cd soils followed by communities in the low Cd soil at day 41. In the pH 7.3 soil, climate-driven separation happened around day 7 for moderate and high Cd contents and started to occur slightly for the low Cd soil from day 12 onward.

Soil carbon usage

Porewater organic carbon levels ranged from 15 to 110 mg L^{-1} for all three soils and Cd contents and were not impacted by future climatic conditions (Supplementary Fig. S10). LC-FT-ICR-MS fingerprinting of the organic carbon in the pH 6.3 soil with low and moderate Cd contents revealed a temporal evolution of distinct signatures, with Cd content exerting a stronger influence than climatic condition (Fig. 3). Cadmium amendment increased the mass to charge ratio. It decreased the nominal oxidation state of the remaining carbon from day 35 onward. While future conditions decreased the nominal oxidation state of the remaining carbon at day 67, they did not affect the mass-to-charge ratio. Clustering 640 organic carbon compounds into three size-polarity clusters revealed climatic sensitivity but

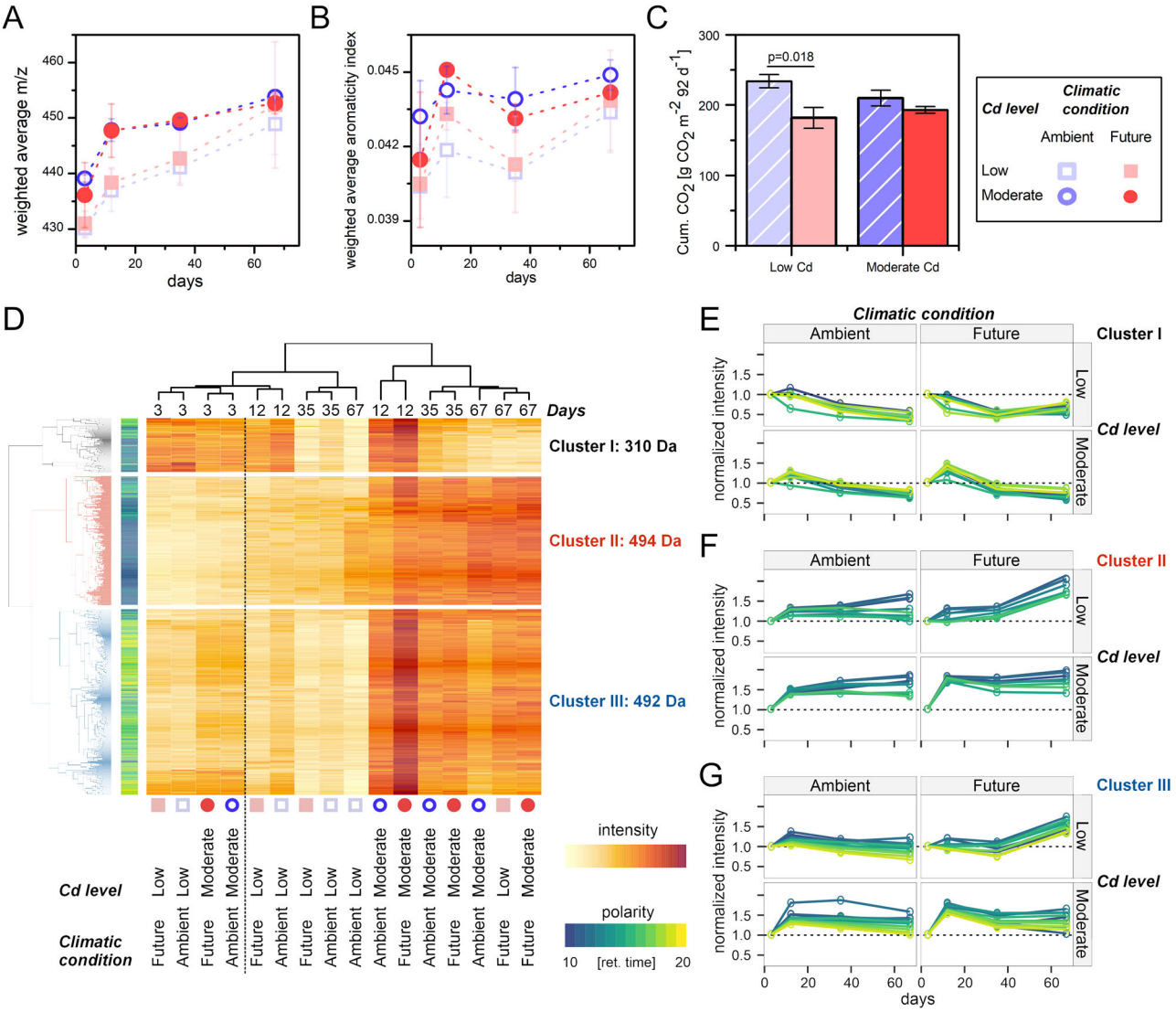

Fig. 3 | Dynamics of porewater organic carbon in an agricultural soil exposed to two climatic conditions. Dissolved organic carbon of the pH 6.3 soil was characterized with LC-FT-ICR-MS at selected time points (days 3, 12, 35, 67). **A** Weighted average mass over charge (m/z) ratio, (**B**) weighted average aromaticity index, and (**C**) corresponding CO_2 emissions for the pH 6.3 soil with a low (154 ± 44 µg kg^{-1} dry soil) and moderate (486 ± 12 µg kg^{-1} dry soil) Cd content. **D** Clustering of key molecular features ($n = 640$) based on standardized mass peak intensities and Euclidian distances. Cluster I ($n = 78$) contains features of low molecular weight and variable polarity (represented by the RP-LC retention time), Cluster II ($n = 230$) and III ($n = 332$) are molecules with higher mass but contrasting polarity and NOSC. **E–G** Temporal trends of clusters from (**D**) using summed intensities of key features according to their polarity. In each panel the summed intensities are normalized to 1 for each segment at the first sampling day. Soils were exposed to ambient (430 ppm_v CO_2 and ambient temperature) and future (800 ppm_v CO_2 and +4 °C in atmospheric temperature respective to the ambient setup) climatic conditions. Averaged data represents the mean ± standard error of 3 biological replicates or minimum-maximum levels when 2 biological replicates are taken.

not to Cd amendment (Fig. 3D–G). Especially at day 67, clusters 2 and 3 showed a higher normalized intensity but also small differences between climatic conditions earlier on. Carbon usage is reflected in respirational CO_2 output. In the pH 6.3 soil, 210 ± 11 g of CO_2 m^{-2} were emitted within 92 days under low Cd and ambient climatic conditions versus 193 ± 5 g CO_2 m^{-2} 92 d^{-1} under respective future conditions (Fig. 3C, Supplementary Fig. S11, Supplementary Table S8). CO_2 emissions also decreased with Cd amendment in this soil. During the initial weeks of the pH 6.3 soil incubation, with moderate ambient temperatures and less drought stress, future conditions stimulated CO_2 emissions across all Cd-treatments. However, in the later experimental phase during summer with more pronounced drought stress and temperatures above 25 °C[47], there was an overall reduction in soil respiration. In the pH 6.7 soil less CO_2 was emitted from the high compared to the low and moderate Cd soil, though future conditions increased respirational output from the low Cd soil only. Also in the pH 7.3 soil, CO_2 emissions decreased with increased soil Cd and future conditions further decreased respiration for the native and low Cd but enhanced CO_2 emissions for the high Cd.

Soil nitrogen cycling

Porewater ammonium and nitrate concentrations in the pH 6.3 soil remained below 0.4 mg L^{-1} and 80 mg L^{-1} for all Cd contents and climatic conditions, respectively, with similar trends in the pH 6.7 soil and no changes in the pH 7.3 soil (Fig. 4, Supplementary Figs. S12, 13). Future conditions resulted in decreased porewater ammonium and 1.8-fold higher nitrate under all three Cd contents after 50 days. N_2O emissions almost significantly decreased due to the presence of more Cd in the pH 6.3 soil and even further under future climatic conditions (Supplementary Fig. S11D–F, Supplementary Table S9). In the pH 6.7 soil, ANOVA indicated a strong interaction between climate and soil Cd at the 95% confidence level (Supplementary Table S9). The exemplary ammonium-oxidizing microorganism *Bacilliae* increased its active relative abundance 1.2-fold under future

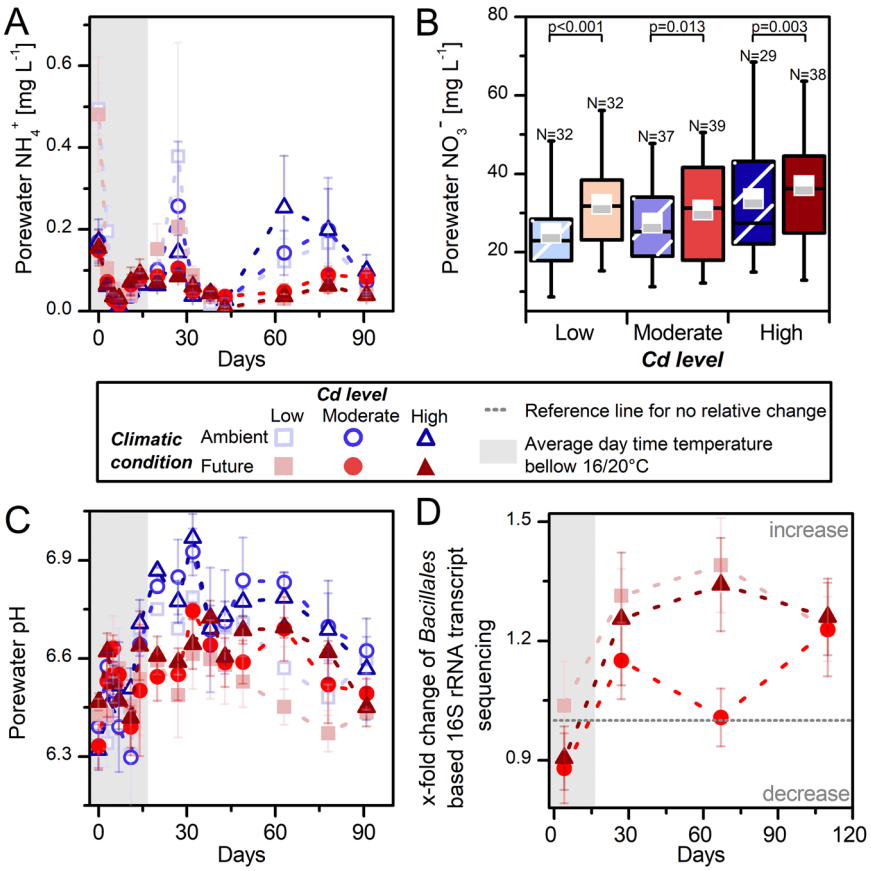

Fig. 4 | Snapshot of microbial nitrogen cycling in the pH 6.3 soil exposed to different climatic conditions. A Porewater ammonium (NH_4^+), (**B**) porewater nitrate (NO_3^-), (**C**) porewater pH for the pH 6.3 agricultural soil, bearing three different total Cd contents (low (squares), moderate (circles), and high (triangles), for exact Cd contents per soil see Supplementary Table S1) and (**D**), relative potential activity changes of the ammonium-oxidizer *Bacillales* based on 16S rRNA transcript sequencing. The soils were exposed to ambient (430 ppm_v CO_2 and ambient temperature) (blue, open/striped symbols) and future (800 ppm_v CO_2 and +4 °C in atmospheric temperature respective to the ambient setup) (red, filled symbols) climatic conditions. Relative changes of the potential activity to microbial groups are based on 16S rRNA transcript sequencing and are calculated relative to the equivalent Cd concentration under ambient climatic conditions. Biological replicates = 5, error bars represent the standard error. N represents the number of datapoints per whisker plot. Significant differences are indicated with *p*-values above plots.

respective to today's conditions. In connection with ammonium oxidation, which liberated protons, the pH of the pH 6.3 soil stabilized between 6.3 and 6.8 during incubation and was reduced by 0.2 pH units for all Cd contents under future climatic conditions (Fig. 4C, Supplementary Fig. S14). A similar trend with a 0.1 pH unit decrease was observed for the pH 6.7 soil under low and moderate Cd contents, and no difference in the pH 7.3 soil.

Discussion and Implications

Future climatic conditions, featuring doubled atmospheric CO_2, 4 °C temperature increase, and reduced soil moisture, notably increased porewater Cd in soils with pH below 7 (scheme in Fig. 5). This interactive effect between soil Cd and climatic conditions (Supplementary Table S10) occurred in native low Cd soils and Cd-amended soils at concentrations relevant to agricultural and industrial contamination scenario[13,30,31]. The heightened Cd bioavailability reflected in free Cd^{2+} increases and extends to deeper mineral-associated fractions, impacting HCl-extractable Cd and altering Cd binding from oxide minerals to organic matter. Thus, it may hold relevance for plant uptake[48].

The observed changes in Cd mobility were season-dependent, prominent during the transition from spring to summer with temperatures exceeding 20 °C in pH 6.3 and 6.7 soils. Despite higher temperatures enhancing Cd adsorption-capacity on minerals[49], they can also increase chemical reactions in the soil and therefore enhance weathering of minerals[50] that have Cd either adsorbed or incorporated in their crystal structure. However, since a drop in pH and increased porewater Cd (Supplementary Fig. S3 A–E) occur simultaneously, the rise in porewater Cd is primarily attributed to soil acidification. This conclusion is further reinforced by a principal component analysis of the geochemical porewater parameters, which reveals a positive correlation between NO_3^- and Cd, and a negative correlation of both NO_3^- and Cd with porewater pH (Supplementary Fig. S15). The PCA results indicate that the nitrogen cycle plays a pivotal role in regulating soil pH under future climatic conditions (Supplementary Fig. S15), and minorly the dissolution of doubled atmospheric CO_2 in soil solution[51]. Ammonium-oxidizing microorganisms, like *Bacilliae*, were stimulated under future conditions (Fig. 4D), leading to increased NH_4^+ turnover to NO_3^- (Fig. 4A, B). This process released protons (Fig. 4C), facilitating cation exchange with mineral surface-bound Cd. Released Cd most likely manifested to equal degrees in the free Cd^{2+} and DOC-associated fraction (Supplementary Table S3), indicating that partitioning between DOC associated and free Cd^{2+} is climate insensitive once climate generally released more Cd into the porewater. Agricultural soils with a more acidic pH than 6.3 could feature such a high mobility of Cd[36], that they may prove to be climate insensitive. However, the used empirical geochemical model[42] is based on sodium and DOC concentrations, as well as solution pH, but it does not account for DOC composition. As a result, it may overestimate the free Cd^{2+} fraction and should be considered an approximation. In soils with high carbonate contents (e.g. pH 7.3 soil with 0.3 $\%_w$ inorganic carbon), cadmium mobilization was limited by the carbonate buffer system capturing protons. Additionally, cadmium associates and integrates more with carbonates, forming calcite-otavite ($Ca\text{-}CdCO_3$) mixed minerals[52], rather than binding to silicate and oxide mineral surfaces as known for lower pH soils[18,53]. Given that approximately 30% of global soils have a pH above 7.3[34,35], climatic change is less likely to affect Cd partitioning in these soils. This proof of concept study covered soils from pH 7.3 to 6.3, representing a pH range, relevant for crop production[34], but missing global soils beyond this range.

Shifts in microbial community taxonomy, diversity, metabolisms, and activity were induced by climatic stressors, influencing observed changes in Cd mobility. The introduction of Cd into the soil, followed by a 14-week acclimatization period, led to distinct microbial communities upon the onset of climate incubation (Fig. 2). The presence or absence of Cd-tolerance genes[54] likely caused this divergence, decreasing activity or cell death among non-tolerant microbial members. As a result, lysed non-Cd-tolerant cells became a primary food and energy source for surviving microbes, while cell

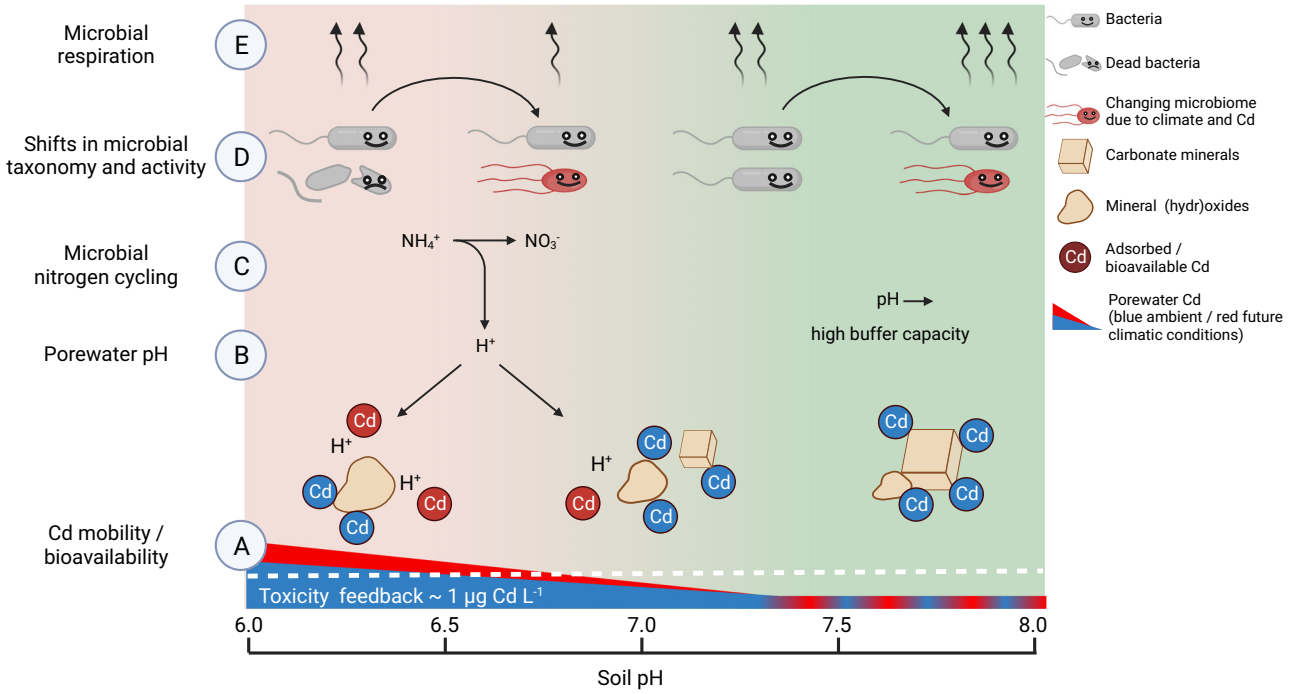

Fig. 5 | Scheme illustrating climate change impacts on soil Cd bioavailability with subsequent implications for microbiome dynamics. A Future climatic conditions increase porewater and bioavailable Cd in acidic but not in alkaline soils as indicated by blue colors for ambient and red colors for future climatic conditions (**B**) through alterations in soil pH upon climate-driven differences in microbial activity such as ammonium oxidation (**C**), cell death (indicated by broke bacteria), and altered taxonomic and active microbial composition (**D**) (indicated by different colors and shapes of bacteria). Porewater Cd concentrations below approximately 1 µg L^{-1} have a stimulatory effect on the soil microbiome (**E**), most prominent for neutral to alkaline soils. At porewater Cd concentrations above approximately 1 µg L^{-1}, stimulatory Cd effects on the microbiome may be outweighed by toxic effects, which is most prominent for soils with a pH < 7 or with high total Cd contents. Figure was created with BioRender.com.

walls and other microbially derived compounds with slower turnover were enriched[55,56]. This process likely contributed to the shift towards larger and more oxidized organic substances (Fig. 3) as also observed in soil profiles[57]. This adaptation allowed the microbial community to reach similar absolute 16S rRNA copy numbers within the 14-week acclimatization period.

Microbial adaption to climatic changes depends on soil history and temperature[58] and is promoted by temperature fluctuations, as implemented in this incubation through natural day and night cycles[59]. However, once future climatic conditions were imposed on the soils, compositional differences in taxonomic and potentially active microbial diversity continued evolving for all soils, as indicated by soil-specific movements on PCoA 1 and 2 coordinates until the end of incubation. While we implemented sudden climatic changes in this study, which may not fully represent the gradual nature of real-world climate change, the data indicate that the microbial community acclimatized and continued adapting to these changes as expected (Fig. 2). These differences first appeared at different time points in each soil depending on transitions to summertime temperatures, under which higher Cd mobilities were observed. Taxonomic changes in the total and potentially active microbiome were less rapid and pronounced under different climates than Cd amendment. The 4 °C climate differences had a more interfering impact on microbial activity and function rather than survival contrasting the drastic effects of Cd amendment. Upon climate-induced Cd mobilization, microorganisms lacking metal resistance genes were inactivated, and some potentially perished, becoming a carbon source of small and aliphatic substrates for thriving Cd-tolerant microorganisms[1] (Fig. 3). This gradual shift in organic carbon signatures towards higher aromaticity and m/z ratio has implications for the energy content of the soil organic matter.

The potential link between a climate-induced shift in microbiome dynamics and increased soil Cd mobility is evident through similar but less pronounced shifts in PCoA 1 and 2 of native low Cd microbial communities compared to Cd-amended soils (statistically significant average distances of the Bray Curtis dissimilarity relative to the low Cd soil in Supplementary Table S4). Notably, in the pH 7.3 soil, the microbial community responded firmly even to low amounts of added Cd. While future climatic conditions did not impact porewater nor bioavailable Cd, they promoted changes in microbiome dissimilarity from day seven onwards for the moderate and high Cd treatment, followed later by the low Cd soil. This suggests that an interaction between climatic conditions and elevated Cd levels in these soils stimulated the microbiome to adapt sooner than when only climatic conditions were applied.

The overall porewater Cd level was crucial in determining whether climate-affected Cd stimulated[8,9,16,60] or adversely impacted[16–18] microbiome balance and functioning. In soils where porewater Cd remained below approximately 0.8 to 1 µg L^{-1} (non-grey shaded data in Fig. 1), microbial diversity adapted, and activity was stimulated, as indicated by low impacts on Faith phylogenetic diversity (Supplementary Table S15, 16) and increased CO_2 and N_2O emissions (Fig. 4). Conversely, when porewater Cd exceeded approximately 1 µg L^{-1}, notably in highly contaminated soils or those with pH < 7, cadmium reached toxic levels, reducing initial microbiome phylogenetic diversity, which later recovered. Broad changes in microbiome dissimilarity (Fig. 2) along with the shift toward larger and oxidized organic molecules (Fig. 3) suggest that dying microorganisms served as a food source for a subsequently thriving microbiome with specialized metabolic pathways[55]. In the specific light of the nitrogen cycle in the pH 6.3 soil, climate-induced Cd mobility increases were associated with increased nitrate due to the increased oxidation of ammonium (Fig. 4) and likely enhanced nitrite oxidation towards nitrate.

Climate's impact on metal mobility in soils holds significant implications, especially in cropland systems. We partially assessed this impact by monitoring CO_2 and N_2O emissions from agricultural soils. With ~30% of global agricultural soils exhibiting a pH > 7[34,35], coupled with the rising trend of nitrogen-based fertilizer application[61], and the substantial radiative forcing of N_2O[21], the potential exists for higher agricultural greenhouse gas

emissions globally than currently anticipated. Accurate projections are crucial given that agriculture contributes 3.7% to anthropogenically-derived greenhouse gas emissions[62]. Conversely, with 70% of global agricultural soils exhibiting pH < 7[34,35], and considering a small fraction of agricultural soils with pH below 6 and thus less likely to be impacted by climate, there is a heightened risk of increased mobile Cd transferring into the food chain even at overall background total soil Cd contents, thereby endangering yields and food quality. While current climate and crop production simulations consider temperature, elevated atmospheric CO_2, and rainfall patterns[21], they neglect the presence and bioavailability of metals in soils. This oversight may exacerbate reduced ecosystem health, groundwater quality, food production, and climate feedback through altered microbiome dynamics.

Material and Methods

Soil preparation and acclimatization

Three agricultural soils from the same parent rock material and the same climatic region were sampled from farms in South-west Germany. Soils were chosen for their difference in $CaCl_2$-based pH and are subsequently named by their pH in this manuscript; soil with pH 6.3 (Tuebingen), soil with pH 6.7 (Dusslingen), and soil with pH 7.3 (Ehningen) (Supplementary Table S1). According to Bradl et al. 2004, increased partitioning of Cd into the porewater is especially relevant for soils with a pH from 5.5 to 7 as Cd mobility drastically changes from almost everything mobile to immobilized through adsorption to organic matter, minerals and incorporation into mineral structures[36]. We confirmed this with a geochemical model for free Cd^{2+} in the porewater[42], suggesting that up to 96% of the dissolved Cd are present as free Cd^{2+} available for plants[48] in the pH 6.3 soil while in the pH 7.3 soil only 60% are present as free Cd^{2+}. At pH below ~5.5, most Cd is expected to be dissolved; therefore, climatic effects are less likely to imprint.

To characterize the soil, soil pH was determined with 2 g of air-dried soils in 10 mL of 0.01 M $CaCl_2$ solution after 1, 24, and 48 hours. Soil texture was determined by wet-sieving and sedimentation analysis with PARIO soil texture analyzer (Meter, USA). Total (organic) carbon and nitrogen contents were determined on air-dried, ground soils by combustion on a soli TOC cube (Elementar, Germany). Cation exchange capacity was determined from 1 g of wet soil in 25 mL 0.1 M $BaCl_2$ for 4 h (horizontal shaker 150 rpm, filtered through 0.45 µm PES filter), followed by cation quantification with microwave plasma atomic emission spectroscopy (4200 MP-AES, Agilent Technologies, USA). Total elemental contents, exchangeable and bioavailable metal contents were quantified according to standard protocols by aqua-regia-based microwave digestion[63], 0.01 M $CaCl_2$[64] and 0.1 M HCl-extractions[65], respectively, followed by quantification on an Agilent 7900 ICP-MS (instrumental details under porewater analysis). Water-extractable carbon and nitrogen were extracted from 5 g of air-dried soil with 40 mL H_2O for 1 h (horizontal shaker, 150 rpm, filtered through 0.45 µm PES filter)[66]. Organic carbon was quantified on a multi-N/C analyzer (Analytik Jena, Germany) and inorganic nitrogen species on an AutoAnalyzer3 (SEAL Analytical, Germany).

All soils were prepared in the same way for experimental runs. First, the soil was air-dried in the dark at 20 °C and sieved with a 2 mm mesh combined with manual removal of plant and rock material[67]. Subsequently, the soil was mixed and separated into equal parts using a sample splitter (RT 50, Retsch, Germany). Next, soils were rewetted with artificial rainwater containing either $CdCl_2$ (trace metal grade, Sigma Aldrich) for metal-bearing set-ups or with $CaCl_2$ for low-Cd soils to account for chlorine toxicity effects and equal ion amendments. Finally, metal stock solutions were applied with a pressure sprayer and thoroughly mixed with a stirring adapter of a drilling machine. The following Cd amendments were prepared for each soil: low Cd with 2.5 mg Ca kg^{-1} ($CaCl_2$ addition), moderate Cd with the addition of 0.3 mg Cd kg^{-1} ($CdCl_2$), and 2.2 mg Ca kg^{-1} dry soil ($CaCl_2$), and high Cd with the addition of 2.5 mg Cd kg^{-1} dry soil ($CdCl_2$). Soils were acclimated to metal amendments for 14 weeks, allowing Cd to establish a realistic binding environment to the soil matrix[68] and for the soil microbiome to adapt to metal stress[17]. To do so, soils were run through three dry (5 % gravimetric water content) and wet (20 % gravimetric water content) cycles for acclimatization until the start of the experiment.

Experimental set-up

Black PVC-U tubes (inner diameter: 7.3 cm height: 33 cm) (Supplementary Fig. S1), washed with 1 M HCl, MilliQ water and wiped with 80% ethanol, were filled with 800 g of air-dried soil, and randomly distributed in climate-controlled chambers (110 x 50 x 50 cm) made of poly(methyl methacrylate) (front and top) and polyvinylchloride (ground, back and sides). Within each tube, a rhizonsampler (RhizonFlex, 5 mm, 0.22 µm, Rhizosphere Research Products, Netherlands) was installed horizontally, 8 cm below the soil surface (Fig. S1). The three soils were run individually between 2019 to 2021. The replication for each experiment was three, four, and five tubes for pH 7.3, 6.7, and 6.3 soils, respectively, as with each experiment our experience and pipeline in sample handling allowed for more replication. The gravimetric water content of the soil was monitored every five days and weight-adjusted to 25% with autoclaved artificial rainwater. Chambers were placed outside to ensure natural day/night cycles (for detailed climatic conditions, see Supplementary Fig. S2). Each chamber was equipped with a temperature control unit using a raspberry Pi 3b+ (Raspberry Trading., United Kingdom) and DS18B20 T-sensor (Analog-devices, USA) monitoring temperature in four different spots within the chamber in minute intervals. The ambient chambers featured the temperature and 430 ppmv atmospheric CO_2 conditions of the surrounding environment, albeit on average about 2 °C higher than outside due to the greenhouse effect within the chamber (Supplementary Fig. S2). The future chamber implemented future climatic conditions by adding +4 °C and +370 ppmv CO_2 compared to the ambient chamber through heater fans and CO_2 infusion, respectively. When the mean difference in atmospheric temperature inside the ambient and future chambers dropped below 3.9 °C, heating fans (HP8232, Phillips, Germany) re-adjusted the temperature in the future chamber with simultaneous air mixing without heating in the ambient chamber. Increased atmospheric CO_2 concentration was achieved by mixing pumped (HiBlow HAP-100) ambient air with CO_2 (industrial grade 99.5 %, Westfalen Gas, Germany) using a two-tube gas proportioner (ColeParmer, USA) with flow tube 044-40 with stainless steel float (Cole-Parmer) for ambient air and flow tube 042-15 with glass float (Cole-Parmer, USA) for CO_2. The ambient set-up was constructed the same, excluding the CO_2 flow. The flow was 36.6 L min^{-1} for ambient air and 14.66 mL min^{-1} for CO_2. By this, the chamber volume was exchanged eight times per hour.

While climatic-controlled incubation studies allow for evaluating subtle differences in biogeochemical processes, they also pose constraints, such as a potential overestimation of mobilized Cd or greenhouse gas emissions due to the homogenization of soils, amendment of Cd, and lack of horizontal and vertical water flow. By acclimating the soil to Cd inputs for weeks before the experiments, we aimed at a more realistic Cd binding[68] and an adaptation and recovery of the soil microbiome to the sudden stress[20], reflected by porewater Cd concentrations in the expected range of field concentrations[14]. We could not account for an evolutionary adaptation of the microbiome to a changing climate for decades into the future and are constrained to using today's soils with the current microbial community.

Porewater analysis

Porewater was extracted from each column through rhizon sampler using 20 mL syringes (Braun, Germany). Porewater pH was determined directly in technical unicates per soil column in 1.5 mL of extracted soil solution with an InLab Easy pH probe (Mettler Toledo, USA). The remaining porewater was filtered through a 0.22 µm PES filter (pre-washed with 10 mL MilliQ to remove organic carbon impurities). For quantification of dissolved Cd, filtered porewater was diluted and acidified with nitric acid (trace metal grade), stored at 4 °C in darkness, and analyzed in technical triplicates on an Agilent 7900 ICP-MS (samples of pH 6.3 soil) and a Thermo Scientific xSeries 2 ICP-MS (samples of pH 6.7 and 7.3 soil). For both, certified quality controls at different concentrations were measured every 20th sample; for instrumental drifts, Rhodium as an internal standard was used for

corrections. Porewater organic carbon (DOC) and nitrogen species (NO_3^-, NH_4^+) were quantified on a multi N/C 2100 (Analytik Jena, Germany) and a continuous flow analyzer (AA3, Seal analytical, USA), respectively. Details on LC-FT-ICR-MS analysis are found in *Methods*.

Gas analysis

For determining greenhouse gas emissions from soils, columns were closed air-tight with rubber stoppers (64.5–75.5, Deutsch Neumann, Germany) from outside the chambers by leveling down screw rods. A cannula was passed through the plug and connected to Tygon tubing (ID 1 mm, Ismatec), which ended at a 3-way valve (Braun, Germany) with two syringes. A sample was drawn with one syringe to flush Tygon tubes with headspace gas, and the sample was discarded. Subsequently, a headspace gas sample was drawn with the other syringe after 0, 15, and 30 min and injected into helium-flushed 20 mL crimped headspace vials. In total, 5% of the gas headspace was removed. After sampling, tubes were opened again, allowing the headspace to be exchanged passively by air circulation and diffusion. Gas samples were analyzed immediately after sampling on a TraceGC1300 (ThermoFisher Scientific, modified by S + HA analytics, Germany), in which the sample is split into two different column configurations (first configuration: 30 m long, 0.53 mm ID TGBondQ column and 30 m long, 0.53 mm ID Molsieve column; second configuration: 30 m long, 0.53 mm ID TGBondQ column and a 30 m long 0.25 mm ID TGBondQ+ column (all ThermoFisher Scientific, USA), each connected to a Pulse Discharged Detectors. This allowed the simultaneous quantification of CO_2, N_2O, and CH4. Gas concentrations were quantified with external calibrations, and gas fluxes were calculated by linear regression and cumulated throughout the experiment. The cumulation was only performed for 12 h per day, as fewer greenhouse gas emissions are expected during the night, which are not included in the cumulative data. For the entire experiment, CH_4 emissions were below the detection limit.

Soil sampling

Soil was sampled from the top 5 cm of soil in each column throughout the experiment. Soil was homogenized with a sterile spatula (baked at 300 °C for 3 h) and aliquoted into a sterile 2 mL microcentrifuge tube (Eppendorf, Germany) for molecular ecology analysis, into a 15 mL centrifuge tube for geochemical analysis, and a 2 mL microcentrifuge tube for water content determinations. Geochemical samples were stored at −20 °C if samples were not processed immediately. Samples for molecular ecology analysis were stored at −80 °C. Soil selective extractions were performed to tease out Cd binding differences due to climatic impacts and included 0.1 M HCl (all soils) and 0.01 M $CaCl_2$ (only pH 6.3 soil) extractants. To do so, 1 g of fresh soil was extracted with 9 mL of the respective extractant for 30 min (0.1 M HCl) or 60 min (0.01 M $CaCl_2$) by 140 rpm horizontal shaking at room temperature in darkness. Supernatants containing extracted elements were collected after centrifugation at 7000 g for 5 min, 0.22 µm filtration, diluted in 2% nitric acid, and stored at 4 °C and darkness until measurement on an Agilent 7900 ICP-MS.

Extended X-ray absorption fine structure analysis

To identify Cd binding environments, soil samples were frozen, freeze-dried, ground, and stored anoxically until measurement. Samples were placed in aluminum sample holders (window 3 mm by 13 mm) and sealed with 0.5 mil Kapton tape from both sides. Cadmium K-edge extended X-ray absorption fine structure (EXAFS) data were obtained at beamline 11-2 and 7-2 at the Stanford Synchrotron Radiation Lightsource (SSRL), Menlo Park, USA. Due to the low Cd concentrations, measurements were conducted using only the high soil Cd samples. Additionally, up to 29 scans per sample were performed to minimize noise and ensure accuracy. To overcome the low Cd levels Spectra were calibrated against a Cd-foil, aligned, and merged subsequently in Athena. Linear combination fittings were performed in Athena with all samples and standards (Supplementary Table S11).

Microbial community assessments

DNA/RNA were co-extracted from 0.6 g of wet soil with a phenol/chloroform/isoamyl alcohol phase separation extraction[69]. The DNA/RNA pellet was dissolved in a 100 µL TE buffer. DNA and RNA contents were quantified with a Qubit 2.0 fluorometer (Thermo Fischer Scientific), quality checked for 260/280 ratios on NanoDrop (Thermo Fisher Scientific), and aliquots were stored at −80 °C. For rRNA analysis, the extracts were purified from DNA with the InvitrogenTM TURBO DNA-freeTM Kit (Thermo Fisher Scientific) and reversely transcribed into complementary DNA (cDNA) using the InvitrogenTM SuperScriptTM III Reverse Transcriptase Kit (Thermo Fischer Scientific). A PCR followed by a 1% (w/v) ethidium-bromide-died agarose gel was performed to check successful DNA removal and subsequent cDNA synthesis.

Gene and transcript copy numbers were quantified with quantitative PCR (qPCR) using 1× SsoAdvanced Universal SYBR Green Supermix (Bio-Rad Laboratories, Hercules, CA, USA). In a 10 µL reaction volume, 1 µL of template DNA (~4 ng) and cDNA (~ 0.5 ng) or a tenfold dilution series of the standard plasmid DNA were annealed with 125 nM of primers 515-F (5′-GTGYCAGCMGCCGCGGTAA-3′)[70] and 806-R (5′-GGACTAC NVGGGTWTCTAAT-3′)[71] and 5% DMSO. As standard, a 16S rRNA Thiomonas gene fragment was amplified. The qPCR program ran on the CFX Connect Real-Time PCR Detection System (Bio-Rad Laboratories, Hercules, USA) with 3 min at 95 °C, 40 cycles of 10 s at 95 °C and 30 s at 55 °C, followed by melting curve analysis. The data analysis was performed using the Bio-Rad CFX Maestro software (Bio-Rad Laboratories, Hercules, USA).

Microbial 16S rRNA genes and transcripts were amplicon-sequenced using primers 515 F and 806R[72]. Quality and quantity of the purified amplicons were determined using agarose gel electrophoresis. Subsequent library preparation steps (Nextera, Illumina, USA) and sequencing were performed using the 2 × 250 bp MiSeq Reagent Kit v2 on an Illumina MiSeq sequencing system (Illumina, San Diego, USA). Adapters were trimmed using the MiSeq Reporter Software. Reconstruction of 16S rRNA gene and transcript sequences and taxonomic annotation was performed with QIIME2 version 2019.10.0[73]. Initially, data from the three sequencing runs were treated separately and merged for each experiment after annotation. Adapter-free sequences were imported into QIIME2 version 2019.10.0, processed with DADA2 version 1.10.0[74] to eliminate PhiX contamination, trim reads (before the median quality drops below 30), merge read pairs, and remove PCR chimeras. Alpha rarefaction curves were produced with the QIIME2 diversity alpha-rarefaction plugin, indicating that the samples' richness had been fully observed (Supplementary Table S12). A Naive Bayes classifier was fitted with 16S rRNA gene sequences extracted with the PCR primer sequences from the QIIME compatible, 99%-identity clustered SILVA v132 database[75]. ASVs were classified by taxon using the fitted classifier[76]. Relative abundance per sample and the remaining ASVs were extracted using the feature table.

Before alpha and beta diversity analyses, the data were rarefied using a specific sampling depth for each experiment. Diversity metrics (alpha diversity: Shannon index, Pielou's evenness, and observed ASVs; beta-diversity: Bray-Curtis dissimilarity) were calculated using the core-diversity and emperor plugins within QIIME2 (Supplementary Tables S13–18).

LC-FT-ICR-MS. Original filtered porewater samples from the pH 6.3 treatments with low (three replicates) and moderate Cd (two replicates) and four time points (days 3, 12, 35, 67) were stored at −20 °C until analysis. After thawing, samples were filtered with 0.2 µm regenerated cellulose filters (Minisart RC4, Sartorius, Germany) before directly injecting 100 µL into a UPLC system coupled to an FT-ICR-MS. The method was adapted from Han et al. [77] and is suitable to separate and detect dissolved organic matter. Briefly, the chromatographic separation was performed on reversed phase polar end-capped C18 column (ACQUITY HSS T3, 1.8 µm, 100 Å, 150 × 3 mm, Waters, Milford, MA) equipped with guard column (ACQUITY UPLC HSS T3 VanGuard Precolumn, 100 Å, 1.8 µm, 2.1 mm × 5 mm, Waters). An FT-ICR mass

spectrometer equipped with a dynamically harmonized analyzer cell (solariX XR, Bruker Daltonics Inc., Billerica, MA, USA) and a 12 T refrigerated actively shielded superconducting magnet (Bruker Biospin, Wissembourg, France) was coupled to the LC system. An electronspray ionization source (Apollo II, Bruker Daltonics Inc., Billerica, MA, USA) was used in negative mode (capillary voltage: 4.3 kV, nebulizer gas pressure: 1.0 bar, dry gas temperature: 250 °C, dry gas flow rate: 8.0 L/min). Mass spectra for LC-MS measurements were acquired in broadband mode (147.41 to 1000 m/z) with a transient size of 2 MWord(~0.84 s FID) and full profile mode. The ion accumulation time (IAT) was set to 8 ms.

DOM from the porewater eluted between 9.8 and 19.9 min. The LC-FT-ICR-MS chromatogram were segmented into 1 min bins, resulting in 12 segments per sample (nSamples = 40). Each segment was treated as an individual spectrum and internally calibrated (DataAnalysis 5.0, Bruker Daltonics) with masses commonly found in DOM (m/z 150–1000, n calibrants > 186). Assuming singly charged ions (based on 12C–13 C1 m/z spacing), molecular formulas (MFs) were assigned to each m/z value with a signal/noise ratio > 4 in the mass range m/z 150–1000 using an in-house software considering the following elements 12C0–60, 13C0–1, 1H0–122, 16O0–40, 14N0–2, 32S0–1, 34S0–1 and a maximum assignment error of <abs(0.5) ppm. Only formulas with $0.3 \le H/C \le 2.5$, $0 \le O/C \le 1$, $0 \le N/C \le 0.5$, $0 \le DBE \le 20$ (double bound equivalent, DBE = 1 + 0.5 * (2 c - h + n) and $-10 \le DBE\text{-}O \le +10$ were considered for further data evaluation[78,79]. Isotopologue formulas (13C, 34S) were used for quality control but removed from the final data set as they represent duplicate chemical information. All MF found in blanks (ultrapure water measured with LC-FT-ICR-MS, n Blanks = 4) were removed from the corresponding segments in the samples.

Based on the mass peak magnitudes of all assigned peaks, intensity-weighted mean (wa) molecular descriptors were calculated for aromaticity index (AI = [1 + c - o - s − 0.5 * (h + n)] / [c - o - s – n])[80], nominal oxidation state of carbon (NOSC = 4 – [4c + h − 3n − 2o + 5p − 2 s] / c) and m/z according to waX = ∑(Xi * Intensity) / ∑(Intensity), where X is a molecular descriptor, and i is the i-th assigned peak in the spectrum.

For Fig. 3A, B, all segments of a respective biological replicate were averaged into a single spectrum considering MF which occurred at least in two segments, with average peak magnitudes calculated as simple means, and weighted average molecular descriptors calculated as above. For Fig. 3D-G, key features were extracted from the data set as follows: First, each segment of the biological replicates was averaged using only MF occurring in all replicates, and which have a peak magnitude variability (calculated as median +− IQR from 2-3 replicates) < 20%, resulting in 12 segments per sample and 12970 unique MF. Second, MF were extracted from each segment which show a peak magnitude variability (calculated as coefficient of variance from 40 samples) > 25%, resulting in 640 key features (MFxSegment, $14 \le n \le 116$ key features per segment and 563 unique MF) for the entire data set. Key features thus represent MF, which show the largest differences within the data set.

Data analysis

Mean and standard errors were calculated for all data sets. Interactions between climatic conditions and Cd were evaluated using a two-factorial ANOVA at a 95% confidence interval, specifically for the greenhouse gas emissions data. Differences between individual treatments were assessed with a Student's t-test at a 95% confidence interval. To analyze porewater Cd mobility, a generalized mixed linear model was employed, with climatic conditions, time, and soil Cd levels treated as fixed factors. To address which factors influenced porewater Cd mobility a principle component analysis was performed on the geochemical porewater data. For the microbial dissimilarity, a principle coordinates analysis was performed based on the Bray-Curtis dissimilarity of the 16S rRNA gene and transcript amplicon sequencing. LC-FT-ICR-MS key features were clustered based on Euclidian distance and complete clustering using the *heatmap* function in R (version 4.3.0).

Reporting summary

Further information on experimental design is available in the Nature Research Reporting Summary linked to this paper.

Data availability

The data that support the findings of this study are included in a compressed Source Data file at figshare (https://doi.org/10.6084/m9.figshare.27165732.v1), FT-ICR-MS data is available via the UFZ data depository (10.48758/ufz.14199) and raw sequencing data were deposited at the Sequence Reads Archive (SRA, BioProject: PRJNA1022319, (https://www.ncbi.nlm.nih.gov/bioproject/PRJNA-1022319).

Received: 14 May 2024; Accepted: 16 October 2024;
Published online: 30 October 2024

References

1. Bastida, F. et al. Global ecological predictors of the soil priming effect. *Nat. Commun.* **10**, 3481 (2019).
2. Du, Y. et al. Elevated carbon dioxide stimulates nitrous oxide emission in agricultural soils: A global meta-analysis. *Pedosphere* **32**, 3–14 (2022).
3. Lehmann, J., Bossio, D. A., Kogel-Knabner, I. & Rillig, M. C. The concept and future prospects of soil health. *Nat. Rev. Earth Environ.* **1**, 544–553 (2020).
4. Nielsen, M. N., Winding, A., Binnerup, S. & Hansen, B. Microorganisms as indicators of soil health. (National Environmental Research Institute, Denmark., 2002).
5. Oliverio, A. M., Bradford, M. A. & Fierer, N. Identifying the microbial taxa that consistently respond to soil warming across time and space. *Glob. Chang Biol.* **23**, 2117–2129 (2017).
6. Rustad, L. et al. A meta-analysis of the response of soil respiration, net nitrogen mineralization, and aboveground plant growth to experimental ecosystem warming. *Oecologia* **126**, 543–562 (2001).
7. Schindlbacher, A. et al. Soil respiration under climate change: prolonged summer drought offsets soil warming effects. *Glob. Change Biol.* **18**, 2270–2279 (2012).
8. Shi, W. & Ma, X. Effects of heavy metal Cd pollution on microbial activities in soil. *Ann. Agric Environ. Med* **24**, 722–725 (2017).
9. Xu, Y. et al. Microbial functional diversity and carbon use feedback in soils as affected by heavy metals. *Environ. Int* **125**, 478–488 (2019).
10. Pretty, J. et al. Global assessment of agricultural system redesign for sustainable intensification. *Nat. Sustainability* **1**, 441–446 (2018).
11. Jansson, J. K. & Hofmockel, K. S. Soil microbiomes and climate change. *Nat. Rev. Microbiol* **18**, 35–46 (2020).
12. Naz, M. et al. The soil pH and heavy metals revealed their impact on soil microbial community. *J. Environ. Manag.* **321**, 115770 (2022).
13. Birke, M. et al. GEMAS: Cadmium distribution and its sources in agricultural and grazing land soil of Europe — Original data versus clr-transformed data. *J. Geochem. Exploration* **173**, 13–30 (2017).
14. Kubier, A., Wilkin, R. T. & Pichler, T. Cadmium in soils and groundwater: A review. *Appl Geochem* **108**, 1–16 (2019).
15. McLaughlin, M. J. & Singh, B. R. in *Cadmium in soils and plants* 1-9 (Springer, 1999).
16. Hou, R. et al. Effect of immobilizing reagents on soil Cd and Pb lability under freeze-thaw cycles: Implications for sustainable agricultural management in seasonally frozen land. *Environ. Int* **144**, 106040 (2020).
17. Khan, S., Hesham, Ael-L., Qiao, M., Rehman, S. & He, J. Z. Effects of Cd and Pb on soil microbial community structure and activities. *Environ. Sci. Pollut. Res. Int.* **17**, 288–296 (2010).
18. Vig, K., Sethunathan, N. & Naidu, R. Bioavailability and toxicity of cadmium to microorganisms and their activities in soil: a review. *Adv. Environ. Res.* **8**, 121–135 (2003).

19. Lu, M., Xu, K. & Chen, J. Effect of pyrene and cadmium on microbial activity and community structure in soil. *Chemosphere* **91**, 491–497 (2013).
20. Shahid, M., Dumat, C., Khalid, S., Niazi, N. K. & Antunes, P. M. Cadmium bioavailability, uptake, toxicity and detoxification in soil-plant system. *Rev. Environ. Contamination Toxicol.* **241**, 73–137 (2017).
21. IPCC. Climate Change 2022, Mitigation of Climate Change **6th Asessment Report** (2022).
22. Lasaga, A. C. Chemical kinetics of water-rock interactions. *J. Geophys. Res.: Solid Earth* **89**, 4009–4025 (1984).
23. Adhikari, T. & Singh, M. Sorption characteristics of lead and cadmium in some soils of India. *Geoderma* **114**, 81–92 (2003).
24. Li, X., Zhou, Q., Wei, S., Ren, W. & Sun, X. Adsorption and desorption of carbendazim and cadmium in typical soils in northeastern China as affected by temperature. *Geoderma* **160**, 347–354 (2011).
25. Bradford, M. A. et al. Cross-biome patterns in soil microbial respiration predictable from evolutionary theory on thermal adaptation. *Nat. Ecol. Evol.* **3**, 223–231 (2019).
26. van Groenigen, K. J., Osenberg, C. W. & Hungate, B. A. Increased soil emissions of potent greenhouse gases under increased atmospheric CO_2. *Nature* **475**, 214–216 (2011).
27. Sun, X. et al. Effect of rice-straw biochar on nitrous oxide emissions from paddy soils under elevated CO2 and temperature. *Sci. total Environ.* **628**, 1009–1016 (2018).
28. Banerjee, S. & van der Heijden, M. G. A. Soil microbiomes and one health. *Nat. Rev. Microbiol.* **21**, 6–20 (2023).
29. Rillig, M. C. et al. The role of multiple global change factors in driving soil functions and microbial biodiversity. *Science* **366**, 886–890 (2019).
30. Smith, D. B., Solano, F., Woodruff, L. G., Cannon, W. F. & Ellefsen, K. J. Geochemical and mineralogical maps, with interpretation, for soils of the conterminous United States. *Scientific Investigations Report-US Geological Survey*, https://doi.org/10.3133/sir20175118 (2019).
31. Shi, T. et al. Status of cadmium accumulation in agricultural soils across China (1975–2016): From temporal and spatial variations to risk assessment. *Chemosphere* **230**, 136–143 (2019).
32. McCauley, A., Jones, C. & Jacobsen, J. Soil pH and organic matter. *Nutrient Manag. Modul.* **8**, 1–12 (2009).
33. Holland, J. E. et al. Liming impacts on soils, crops and biodiversity in the UK: A review. *Sci. total Environ.* **610**, 316–332 (2018).
34. Batjes, N. *A global data set of soil pH properties*. (International Soil Reference and Information Centre, 1995).
35. Sposito, G. in *Encyclopedia Britannica* (https://www.britannica.com/science/soil, 2024).
36. Bradl, H. B. Adsorption of heavy metal ions on soils and soils constituents. *J. Colloid Interface Sci.* **277**, 1–18 (2004).
37. Kottek, M., Grieser, J., Beck, C., Rudolf, B. & Rubel, F. World map of the Köppen-Geiger climate classification updated. *Meteorologische Z.* **15**, 259–263 (2006).
38. IPCC. *Climate change 2013: the physical science basis: Working Group I contribution to the Fifth assessment report of the Intergovernmental Panel on Climate Change*. (Cambridge university press, 2013).
39. Le Quéré, C. et al. Global Carbon Budget 2018. *Earth Syst. Sci. Data* **10**, 2141–2194 (2018).
40. Schwalm, C. R., Glendon, S. & Duffy, P. B. RCP8.5 tracks cumulative CO(2) emissions. *Proc. Natl Acad. Sci. USA* **117**, 19656–19657 (2020).
41. Liu, P. R. & Raftery, A. E. Country-based rate of emissions reductions should increase by 80% beyond nationally determined contributions to meet the 2 degrees C target. *Commun. Earth Environ.* **2**, https://doi.org/10.1038/s43247-021-00097-8 (2021).
42. Viala, Y., Sappin-Didier, V., Bussiere, S., Coriou, C. & Nguyen, C. Simple models efficiently predict free cadmium Cd(2+) in the solutions of low-contaminated agricultural soils. *Sci. Total Environ.* **778**, 146428 (2021).
43. Kicińska, A., Pomykała, R. & Izquierdo-Diaz, M. Changes in soil pH and mobility of heavy metals in contaminated soils. *Eur. J. Soil Sci.* **73**, https://doi.org/10.1111/ejss.13203 (2021).
44. Ming, H. et al. Competitive sorption of cadmium and zinc in contrasting soils. *Geoderma* **268**, 60–68 (2016).
45. Wu, B. et al. Response of soil micro-ecology to different levels of cadmium in alkaline soil. *Ecotoxicol. Environ. Saf.* **166**, 116–122 (2018).
46. Fajardo, C. et al. Pb, Cd, and Zn soil contamination: monitoring functional and structural impacts on the microbiome. *Appl. Soil Ecol.* **135**, 56–64 (2019).
47. Carey, J. C. et al. Temperature response of soil respiration largely unaltered with experimental warming. *Proc. Natl Acad. Sci. USA* **113**, 13797–13802 (2016).
48. Lin, Z., Schneider, A., Sterckeman, T. & Nguyen, C. Ranking of mechanisms governing the phytoavailability of cadmium in agricultural soils using a mechanistic model. *Plant Soil* **399**, 89–107 (2015).
49. Roth, E., Mancier, V. & Fabre, B. Adsorption of cadmium on different granulometric soil fractions: Influence of organic matter and temperature. *Geoderma* **189-190**, 133–143 (2012).
50. Kump, L. R., Brantley, S. L. & Arthur, M. A. Chemical weathering, atmospheric CO2, and climate. *Annu. Rev. Earth Planet. Sci.* **28**, 611–667 (2000).
51. Ferdush, J. & Paul, V. A review on the possible factors influencing soil inorganic carbon under elevated CO2. *Catena* **204**, 105434 (2021).
52. Muehe, E. M. et al. Organic carbon and reducing conditions lead to cadmium immobilization by secondary Fe mineral formation in a pH-neutral soil. *Environ. Sci. Technol.* **47**, 13430–13439 (2013).
53. Loganathan, P., Vigneswaran, S., Kandasamy, J. & Naidu, R. Cadmium Sorption and Desorption in Soils: A Review. *Crit. Rev. Environ. Sci. Technol.* **42**, 489–533 (2012).
54. Bravo, D. & Braissant, O. Cadmium-tolerant bacteria: current trends and applications in agriculture. *Lett. Appl Microbiol* **74**, 311–333 (2022).
55. Roszak, D. & Colwell, R. Survival strategies of bacteria in the natural environment. *Microbiol. Rev.* **51**, 365–379 (1987).
56. Malik, A. A. et al. Linking molecular size, composition and carbon turnover of extractable soil microbial compounds. *Soil Biol. Biochem.* **100**, 66–73 (2016).
57. Roth, V.-N. et al. Persistence of dissolved organic matter explained by molecular changes during its passage through soil. *Nat. Geosci.* **12**, 755–761 (2019).
58. Bradford, M. A. et al. Thermal adaptation of soil microbial respiration to elevated temperature. *Ecol. Lett.* **11**, 1316–1327 (2008).
59. Zhang, Y. et al. Temperature fluctuation promotes the thermal adaptation of soil microbial respiration. *Nat. Ecol. Evol.* **7**, 205–213 (2023).
60. Duan, C., Liu, Y., Zhang, H., Chen, G. & Song, J. Cadmium pollution impact on the bacterial community of haplic cambisols in Northeast China and inference of resistant genera. *J. Soil Sci. Plant Nutr.* **20**, 1156–1170 (2020).
61. FAO. (Rome, 2022).
62. Klein Goldewijk, K., Beusen, A., Doelman, J. & Stehfest, E. Anthropogenic land use estimates for the Holocene – HYDE 3.2. *Earth Syst. Sci. Data* **9**, 927–953 (2017).
63. Melaku, S., Dams, R. & Moens, L. Determination of trace elements in agricultural soil samples by inductively coupled plasma-mass spectrometry: Microwave acid digestion versus aqua regia extraction. *Analytica Chim. Acta* **543**, 117–123 (2005).
64. Pueyo, M., López-Sánchez, J. & Rauret, G. Assessment of CaCl2, NaNO3 and NH4NO3 extraction procedures for the study of Cd, Cu, Pb and Zn extractability in contaminated soils. *Analytica Chim. acta* **504**, 217–226 (2004).

65. Sabienë, N., Brazauskienë, D. M. & Rimmer, D. Determination of heavy metal mobile forms by different extraction methods. *Ekologija* **1**, 36–41 (2004).
66. Jones, D. & Willett, V. Experimental evaluation of methods to quantify dissolved organic nitrogen (DON) and dissolved organic carbon (DOC) in soil. *Soil Biol. Biochem.* **38**, 991–999 (2006).
67. Adekanmbi, A. A., Shaw, L. J. & Sizmur, T. Effect of Sieving on Ex Situ Soil Respiration of Soils from Three Land Use Types. *J. Soil Sci. Plant Nutr.* **20**, 912–916 (2020).
68. Simpson, S. L., Angel, B. M. & Jolley, D. F. Metal equilibration in laboratory-contaminated (spiked) sediments used for the development of whole-sediment toxicity tests. *Chemosphere* **54**, 597–609 (2004).
69. Lueders, T., Manefield, M. & Friedrich, M. W. Enhanced sensitivity of DNA- and rRNA-based stable isotope probing by fractionation and quantitative analysis of isopycnic centrifugation gradients. *Environ. Microbiol* **6**, 73–78 (2004).
70. Parada, A. E., Needham, D. M. & Fuhrman, J. A. Every base matters: assessing small subunit rRNA primers for marine microbiomes with mock communities, time series and global field samples. *Environ. Microbiol* **18**, 1403–1414 (2016).
71. Apprill, A., McNally, S., Parsons, R. & Weber, L. Minor revision to V4 region SSU rRNA 806R gene primer greatly increases detection of SAR11 bacterioplankton. *Aquat. Microb. Ecol.* **75**, 129–137 (2015).
72. Caporaso, J. G. et al. Global patterns of 16S rRNA diversity at a depth of millions of sequences per sample. *Proc. Natl Acad. Sci.* **108**, 4516–4522 (2011).
73. Bolyen, E. et al. Reproducible, interactive, scalable and extensible microbiome data science using QIIME 2. *Nat. Biotechnol.* **37**, 852–857 (2019).
74. Callahan, B. J. et al. DADA2: High-resolution sample inference from Illumina amplicon data. *Nat. methods* **13**, 581–583 (2016).
75. Pruesse, E. et al. SILVA: a comprehensive online resource for quality checked and aligned ribosomal RNA sequence data compatible with ARB. *Nucleic acids Res.* **35**, 7188–7196 (2007).
76. Bokulich, N. A. et al. Optimizing taxonomic classification of marker-gene amplicon sequences with QIIME 2's q2-feature-classifier plugin. *Microbiome* **6**, 1–17 (2018).
77. Han, L., Kaesler, J., Peng, C., Reemtsma, T. & Lechtenfeld, O. J. Online counter gradient LC-FT-ICR-MS enables detection of highly polar natural organic matter fractions. *Anal. Chem.* **93**, 1740–1748 (2020).
78. Herzsprung, P. et al. Understanding molecular formula assignment of Fourier transform ion cyclotron resonance mass spectrometry data of natural organic matter from a chemical point of view. *Anal. Bioanal. Chem.* **406**, 7977–7987 (2014).
79. Koch, B., Kattner, G., Witt, M. & Passow, U. Molecular insights into the microbial formation of marine dissolved organic matter: recalcitrant or labile? *Biogeosciences* **11**, 4173–4190 (2014).
80. Koch, B. P. & Dittmar, T. From mass to structure: An aromaticity index for high-resolution mass data of natural organic matter. *Rapid Commun. mass Spectrom.* **20**, 926–932 (2006).

Acknowledgements

We thank A. Gloeckle, C. Glotzbach, C. Leven, S. Cafisso, D. Buchner, and the Geomicrobiology group members for help in the laboratory. We also thank F. Schaedler, R. Kallies, and S. Schreiber for their support and advice on sequencing and data evaluation and E. Baeurle, E. Wizemann and J. Bodemer for providing the soil. For FT-ICR-MS measurement, we thank J. Kaesler. We appreciate using the analytical facilities of the Centre for Chemical Microscopy (ProVIS) at the Helmholtz Centre for Environmental Research, Leipzig, which is supported by the European Regional Development Funds (EFRE— Europe funds Saxony) and the Helmholtz Association. This work was financed by the Baden Wuerttemberg Stiftung's Excellence Programme for Postdocs and the Helmholtz Young Investigator Grant RhizoThreats. We further acknowledge infrastructural support by the Deutsche Forschungsgemeinschaft (DFG, German Research Foundation) under Germany's Excellence Strategy, cluster of Excellence EXC2124, project ID 390838134. We thank M. Latimer and R. Davis for beamline support at SSRL (proposal number 5587). Use of the Stanford Synchrotron Radiation Lightsource, SLAC National Accelerator Laboratory, is supported by the U.S. Department of Energy, Office of Science, Office of Basic Energy Sciences under Contract No. DE-AC02-76SF00515. The SSRL Structural Molecular Biology Program is supported by the DOE Office of Biological and Environmental Research and by the National Institutes of Health, National Institute of General Medical Sciences (including P41GM103393). The contents of this publication are solely the responsibility of the authors and do not necessarily represent the official views of NIGMS or NIH.

Author contributions

Funding for this work was acquired by E.M.M.; This work was conceptualized by E.M.M.; Laboratory work was planned by S.D. with primary input from E.M.M. and advised by A.K. and S.F.; Laboratory work was carried out by S.D. and E.B.; Synchrotron work was carried out by S.D., E.M.M., and J.L.P. and analyzed by J.L.P.; Cd quantification was carried out by B.P.F., J.M.L., and S.D.; FT-ICR-MS data were processed by O.L. and S.D.; The manuscript was written by S.D. with primary input from E.M.M. and overall input and discussion from all co-authors.

Funding

Open Access funding enabled and organized by Projekt DEAL.

Competing interests

The authors declare no competing interest.

Additional information

Supplementary information The online version contains supplementary material available at https://doi.org/10.1038/s43247-024-01794-w.

Correspondence and requests for materials should be addressed to E. Marie Muehe.

Peer review information *Communications Earth & Environment* thanks Chaolei Yuan and Mallavarapu Megharaj for their contribution to the peer review of this work. Primary Handling Editors: Alice Drinkwater and Somaparna Ghosh A peer review file is available.